# Flat versus steep subduction: Contrasting modes for the formation and exhumation of high- to ultrahigh-pressure rocks in continental collision zones

Z.H. Li [a,b,c,*], Z.Q. Xu [a], T.V. Gerya [c,d]

[a] Institute of Geology, Chinese Academy of Geological Sciences, 100037 Beijing, China
[b] Department of Earth Sciences, Nanjing University, 210093 Nanjing, China
[c] Institute of Geophysics, ETH-Zurich, 8092 Zurich, Switzerland
[d] Geology Department, Moscow State University, 119899 Moscow, Russia

## ARTICLE INFO

## ABSTRACT

Flat and steep subduction are end-member modes of oceanic subduction zones with flat subduction occurring at about 10% of the modern convergent margins and mainly around the Pacific. Continental (margin) subduction normally follows oceanic subduction with the remarkable event of formation and exhumation of high- to ultrahigh-pressure (HP–UHP) metamorphic rocks in the continental subduction/collision zones. We used 2D thermo-mechanical numerical models to study the contrasting subduction/collision styles as well as the formation and exhumation of HP–UHP rocks in both flat and steep subduction modes. In the reference flat subduction model, the two plates are highly coupled and only HP metamorphic rocks are formed and exhumed. In contrast, the two plates are less coupled and UHP rocks are formed and exhumed in the reference steep subduction model. In addition, faster convergence of the reference flat subduction model produces extrusion of UHP rocks. Slower convergence of the reference flat subduction model results in two-sided subduction/collision. The higher/lower convergence velocities of the reference steep subduction model can both produce exhumation of UHP rocks. A comparison of our numerical results with the Himalayan collisional belt suggests two possible scenarios: (1) A spatially differential subduction/collision model, which indicates that steep subduction dominates in the western Himalaya, while flat subduction dominates in the extensional central Himalaya; and (2) A temporally differential subduction/collision model, which favors earlier continental plate (flat) subduction with high convergence velocity in the western Himalaya, and later (flat) subduction with relatively low convergence velocity in the central Himalaya.

© 2010 Elsevier B.V. All rights reserved.

## 1. Introduction

Oceanic subduction zones can be classified into normal-to-steep (high-angle) and flat (low-angle) subduction styles. Steep (normal) subduction usually has a dip angle of $\geq 30°$ at the top of the upper mantle (e.g., Turcotte and Schubert, 2002), whereas flat subduction is characterized by shallow dip angle and a high degree of coupling between the converging plates. In nature, flat subduction occurs at about 10% of the modern convergent margins and mainly around the Pacific, with the best known present-day examples located beneath western South America, in Peru and central Chile/NW Argentina (e.g., Gutscher et al., 2000a,b; Lallemand et al., 2005). It has been proposed that flat subduction may have been widespread during the early stages in the Earth's history and contributed to the processes of continental growth in the Proterozoic and Archean (Abbott et al., 1994; Vlaar, 1983, 1985). However, the cause of flat subduction is the subject of an active discussion with several possible mechanisms

having been proposed, e.g. the subduction of buoyant anomalies (such as bathymetric highs, aseismic ridges, or oceanic plateaus), rapid absolute motion of the overriding plate, interplate hydrostatic suction, a delay in the basalt to eclogite transition, the curvature of the margin, etc. (e.g. Gutscher et al., 2000b). In addition, several analogue (e.g., Chemenda et al., 2000; Espurt et al., 2008; Martinod et al., 2005) and numerical models (e.g., van Hunen et al., 2002a,b, 2004) have explored the conditions permitting the appearance of flat subduction zones as well as their consequences on overriding plate deformation. As discussed by van Hunen et al. (2004), flat subduction does not necessarily imply buoyant slabs. Other factors, such as overriding plate velocity and slab strength, may also play significant roles in controlling this process.

Continental (margin) subduction normally follows oceanic subduction under the convergent forces of lateral "ridge push" and/or oceanic "slab pull". The remarkable event during early continental collision is the formation and exhumation of high- to ultrahigh-pressure (HP–UHP) metamorphic rocks. Occurrences of UHP terranes around the world have been increasingly recognized with more than 20 UHP terranes documented (e.g., Liou et al., 2004), which have repeatedly invigorated the concepts of deep subduction (>100 km) and exhumation of crustal

* Corresponding author. CNRS Laboratory FAST, Univ Paris-6 and Univ Paris Sud-11, Orsay 91405, France.
E-mail address: lzhhai@gmail.com (Z.H. Li).

materials. Continental subduction/collision and exhumation of HP–UHP rocks are widely investigated with analogue (e.g., Boutelier et al., 2004; Chemenda et al., 1995, 1996) and numerical modeling method (e.g., Beaumont et al., 2001, 2009; Burg and Gerya, 2005; Burov et al., 2001; Gerya et al., 2008; Li and Gerya, 2009; Toussaint et al., 2004b; Warren et al., 2008a,b; Yamato et al., 2007, 2008). The tectonic styles of continental subduction can be either "one-sided" (overriding plate does not subduct) or "two-sided" (both plates subduct together) (Faccenda et al., 2008; Pope and Willett, 1998; Tao and O'Connell, 1992; Warren et al., 2008a), as well as several other possibilities, e.g. thickening, slab break-off, slab drips etc. (e.g., Toussaint et al., 2004a,b). Models of HP–UHP rocks exhumation can be summarized into the following groups: (1) syn-collisional exhumation of a coherent and buoyant crustal slab, with formation of a weak zone at the entrance of the subduction channel (Chemenda et al., 1995, 1996; Li and Gerya, 2009; Toussaint et al., 2004b); (2) episodic ductile extrusion of HP–UHP rocks from the subduction channel to the surface or crustal depths (Beaumont et al., 2001; Warren et al., 2008a); and (3) continuous material circulation in the rheologically weak subduction channel stabilized at the plate interface, with materials exhumed from different depths (Burov et al., 2001; Gerya et al., 2002; Stöckhert and Gerya, 2005; Warren et al., 2008a; Yamato et al., 2007).

The previously-mentioned analogue and numerical models for continental subduction/collision associated with burial and exhumation of crustal rocks are mostly based on the steep (normal) subduction mode. It is unknown therefore what the characteristics of HP–UHP metamorphism and exhumation would be in the flat subduction mode. In order to address this issue, we used 2D thermo-mechanical numerical modeling to study the contrasting subduction/collision styles as well as the formation and exhumation of HP–UHP metamorphic rocks in both the flat and steep subduction modes. In addition, we investigated the sensitivities of the model predictions to the convergence velocity. The numerical model results are compared to the western and central Himalayas as this large, young continental collisional belt shows intriguing contrasts in subduction geometry and exhumation patterns along strike.

## 2. Numerical model design

The numerical simulations are conducted with the 2D code "I2VIS" (Gerya and Yuen, 2003a) based on finite differences and marker-in-cell techniques (see Appendix A.1 for details of the numerical methodology). Large scale models ($4000 \times 670$ km, Fig. 1) are designed for studying the dynamic processes from oceanic subduction to continental collision associated with the formation and exhumation of HP–UHP rocks. The non-uniform $699 \times 134$ rectangular grid is designed with a resolution varying from $2 \times 2$ km in the studied collision zone to $30 \times 30$ km far away from it. The lithological structure of the model is represented by a dense grid of ~7 million active Lagrangian markers used for advecting various material properties and temperature (Gerya et al., 2008; Li et al., 2010).

The velocity boundary conditions (Fig. 1) are free slip at all boundaries except the open lower boundary along which an infinity-like mass-conservative condition is imposed (e.g., Gerya et al., 2008; Li et al., 2010). Infinity-like external free slip conditions along the lower boundary imply free slip condition to be satisfied at ~1000 km below the base of the model (external lower boundary). As for the usual free slip condition, external free slip allows global conservation of mass in the computational domain and is implemented by using the following limitation for velocity components at the lower boundary: $\partial v_x/\partial z = 0$, $\partial v_z/\partial z = -v_z/\Delta z_{external}$, where $\Delta z_{external}$ is the vertical distance from the lower boundary to the external boundary where free slip ($\partial v_x/\partial z = 0$, $v_z = 0$) is satisfied. The subducting plate is pushed rightward by prescribing a constant convergence velocity ($Vx$) in a small internal domain that remains fixed with respect to the Eulerian coordinate (Fig. 1).

In the numerical models, the driving mechanism of subduction is a combination of "plate push" (prescribed rightward convergence velocity) and increasing "slab pull" (temperature-induced density contrast between the subducted lithosphere and surrounding mantle). This type of boundary condition is commonly used in numerical models of subduction and collision (e.g., Burg and Gerya, 2005; Currie et al., 2007; Toussaint et al., 2004b; Warren et al., 2008b; Yamato et al., 2007) and assumes that in the globally confined three-dimensional system of plates, local "external forcing" coming either from different slabs or from different sections of the same laterally non-uniform slab can be significant. As discussed in detail by Li and Gerya (2009), although slab pull is considered the most significant global 3-D driving force in subduction, eliminating the lateral push from 2-D models is not necessarily the most realistic option since in this case the plate will be driven only by the local negative buoyancy generated in exactly the same 2-D section. In contrast, 3-D plate motion is driven by the global negative buoyancy of the plates (e.g. Labrosse and Jaupart, 2007).

Following previous numerical studies for similar geodynamic settings (e.g., Li and Gerya, 2009; Warren et al., 2008a), our numerical models are



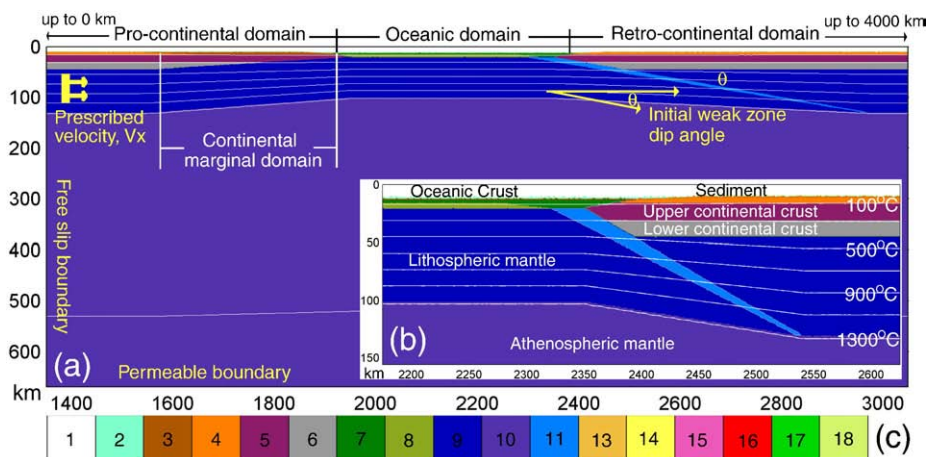**Fig. 1.** Initial model configuration and boundary conditions. a) Enlargement ($1700 \times 670$ km) of the numerical box ($4000 \times 670$ km). Boundary conditions are indicated in yellow. b) The zoomed domain of the subduction zone. White lines are isotherms measured in °C. c) The colorgrid for different rock types, with: 1—air; 2—water; 3,4—sediment; 5—upper continental crust; 6—lower continental crust; 7—upper oceanic crust; 8—lower oceanic crust; 9—lithospheric mantle; 10—athenospheric mantle; 11—weak zone mantle; 13 and 14—partially molten sediment (3 and 4); 15 and 16—partially molten continental crust (5 and 6); 17 and 18—partially molten oceanic crust (7 and 8). The partially molten crustal rocks (13, 14, 15, 16, 17 and 18) are not shown in Figure 1, but will appear during the evolution of the model (e.g., Figs. 3 and 4). In the numerical models, the medium-scale layering usually shares the same physical properties, with different colors used only for visualizing slab deformation and structural development. Detailed properties of different rock types are shown in Tables S2 and S3.

designed with three major domains (from left to right, Fig. 1): (1) a pro-continental domain, (2) an oceanic domain, and (3) a retro-continental domain. The spontaneous deformation of the upper surface of the lithosphere, i.e. topography, is calculated dynamically as an internal free surface by using a low viscosity, initially 10 km thick layer above the upper crust (Fig. 1; see Appendix A1.4 for details). In the continental domain, the initial material field is set up by a 35 km thick continental crust composed of sediment (6 km thick), upper crust (14 km thick) and lower crust (15 km thick), overlying the lithospheric mantle (85 km thick) and subjacent mantle (540 km thick). The oceanic domain comprises an 8 km thick oceanic crust overlying the lithospheric mantle (82 km thick) and subjacent mantle (570 km thick). It is worth noting that the medium scale layering usually shares the same physical properties, e.g. sediment and upper continental crust (Fig. 1; Table S3). The rheology of rocks is composition-, pressure-, temperature- and strain-rate-dependent and accounts for both ductile (at high temperature) and brittle (at low temperature) deformation mechanisms of crustal and mantle rocks (see Appendix A1.2). Detailed properties of different rock types are shown in Tables S2 and S3 in the Appendix (Bittner and Schmeling, 1995; Clauser and Huenges, 1995; Ji and Zhao, 1993; Kirby, 1983; Kirby and Kronenberg, 1987; Ranalli, 1995; Ranalli and Murthy, 1987; Schmidt and Poli, 1998; Turcotte and Schubert, 1982).

The numerical modeling corresponds to the transition from subduction to collision. Slab inclination conditions for these two stages can be strongly dissimilar, which is taken into account by our models in a simplified manner: the initial slab dip angle corresponds to the early subduction stage and the final slab inclination characterizes the later collision stage. In the initial configuration, a rheologically weak zone is imposed (Fig. 1) to define the subduction processes. The weak zone mantle has a wet olivine rheology in contrast to the dry olivine rheology for the mantle elsewhere (Tables S2 and S3), assuming that the current subduction follows a former oceanic subduction channel along which a large amount of water released from the slab formed a weak zone in the mantle (e.g., Gerya and Stöckhert, 2006; Gerya et al., 2002). The prescribed initial dip angle ($\theta$) of the mantle weak zone (Fig. 1) indicates the angle of the former subduction zone. This angle changes spontaneously during further model development with the formation of either flat or steep subduction styles.

The initial thermal structure of continental lithosphere (white lines in Fig. 1) is laterally uniform with 0 °C at the surface (≤10 km depth, the air), 250 °C at 25 km depth, 400 °C at 45 km depth and 1300 °C at the bottom of the lithospheric mantle (130 km depth) (Turcotte and Schubert, 2002). The thermal conditions among these steps are calculated by linear interpolation. The initial thermal structure of oceanic lithosphere (cooling age of 50 Myr) is linearly interpolated with 0 °C at the surface (≤10 km depth) and 1300 °C at the bottom of the lithospheric mantle (100 km depth). The initial temperature gradient in the asthenospheric mantle is around 0.5 °C km$^{-1}$. The thermal boundary conditions have a fixed value (0 °C) for the upper boundary and zero horizontal heat flux across the vertical boundaries. For the lower thermal boundary, an infinity-like external constant temperature condition is imposed, which allows both temperatures and vertical heat fluxes to vary along the permeable box lower boundary, implying that the constant temperature condition is satisfied at ~1000 km below the bottom of the model. This condition is implemented by using the equation $\partial T/\partial z = (T_{external} - T)/\Delta z_{external}$, where $T_{external}$ is the temperature at the external boundary and $\Delta z_{external}$ is the vertical distance from the lower boundary to the external boundary (Gerya et al., 2008; Li et al., 2010).

## 3. Model results

Series of numerical experiments were conducted with variable dip angle of the initial weak zone as well as variable convergence velocity (Table 1). The configurations and parameters are shown in Figure 1 and Tables S1–S3.

### 3.1. Reference flat subduction model

This model has an initial weak zone dip angle ($\theta$) of 10° and a prescribed convergence velocity ($Vx$) of 5 cm yr$^{-1}$ (Model "zfab" in Table 1).

At the initial stages, the relatively strong oceanic plate subducts along the low-angle weak zone to the bottom of the lithospheric mantle (Fig. 2a). The subducting and overriding plates are highly coupled (i.e. interplate hydrostatic suction, Gutscher et al., 2000b; Shemenda, 1993). The subducting plate is then slightly up-bended (Fig. 2b,c) with indenting flatly along the low-viscosity zone at the bottom of the overriding lithosphere (Fig. 2c; see also Figs. S1–S3 in the Appendix for the evolution of density and second invariants of deviatoric strain rate and stress fields). Continued flat subduction leads to the rollback structure and break-off phenomenon at the leading edge of the subducting plate (Fig. 3). The flat subduction style extends for several hundreds to ~1000 kilometers (Fig. 3d).

In the subduction/collision zone, the continental margin subducts following the low-angle oceanic subduction (Fig. 4a) to peak pressure conditions of 1–2.5 GPa (Fig. 4b,c; P–T paths). The continental interior then collides with the overriding plate to form a series of thrust faults in the foreland (Fig. 4b–d). Partial melting occurs in the subduction channel (rheologically weak zone between the strong subducting and overriding plates, which is composed of various subducted crustal rocks and hydrated mantle) under the "bulge" of the overriding plate with peak temperature conditions of 600–800 °C (Fig. 4b,c; P–T paths). Continued continental subduction leads to the extrusion of these partially molten rocks. Finally the HP–HT metamorphic rocks exhume to the surface forming a dome structure near the suture zone (Fig. 4d). In addition, a fold-thrust belt is formed in the foreland extending for about 300–400 km (Fig. 4d). P–T paths (Fig. 4d) show that peak P–T conditions of the exhumed rocks are <2.5 GPa and 600–800 °C, respectively (also see Fig. S4 for the peak pressure and temperature conditions of the collision zone). It indicates these HP metamorphic rocks are formed and exhumed from a depth of less than 80 km.

### 3.2. Reference steep subduction model

This model has an initial weak zone dip angle ($\theta$) of 30° and prescribed convergence velocity ($Vx$) of 5 cm yr$^{-1}$ (Model "zfae" in Table 1).

At the initial stages, the relatively strong oceanic plate subducts along the high angle weak zone to the bottom of the lithospheric mantle (Fig. 5a). Continued subduction of the plate into the asthenospheric mantle triggers small-scale convection in the mantle wedge (Fig. 5b), which further contributes to the decoupling of the two converging plates and the formation of a steep subduction style (Fig. 5c; see also Figs. S5–S7 in the Appendix for the evolution of the

**Table 1**
Description of the numerical experiments.

| Experiments | Initial dip angle ($\theta$) (°) | Convergence velocity ($Vx$) (cm yr$^{-1}$) | Subduction modes | HP/ UHP |
|---|---|---|---|---|
| zfaa | 5 | 5 | Flat | HP |
| zfab | 10 | 5 | Flat | HP |
| zfac | 15 | 5 | Flat | HP |
| zfad | 20 | 5 | Steep | UHP |
| zfae | 30 | 5 | Steep | UHP |
| zfaf | 40 | 5 | Steep | UHP |
| zfag | 50 | 5 | Steep | UHP |
| zfah | 60 | 5 | Steep | UHP |
| zfba | 10 | 10 | Flat | UHP |
| zfbb | 10 | 2.5 | Double/ steep | UHP |
| zfca | 30 | 10 | Steep | UHP |
| zfcb | 30 | 2.5 | Steep | UHP |

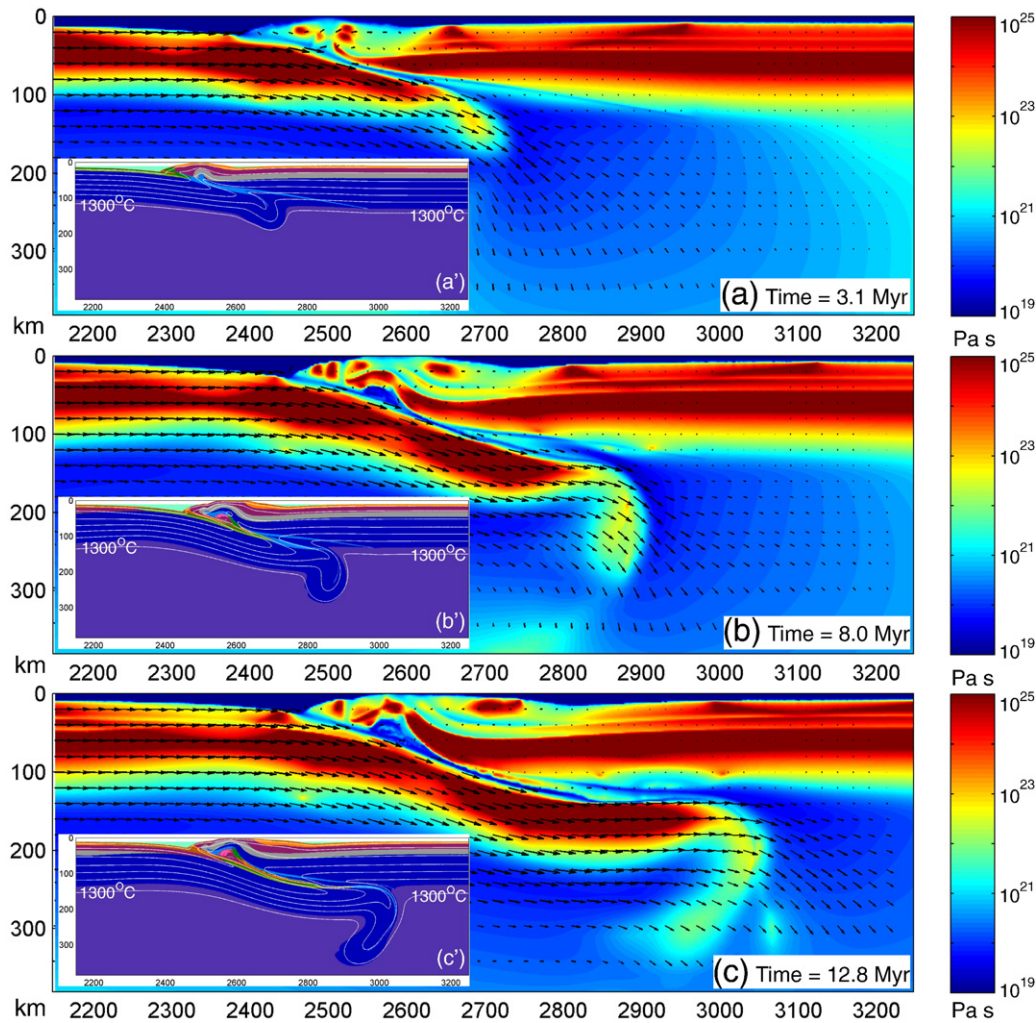All the other parameters are shown in Tables S1–S3 in Appendix A.

**Fig. 2.** Initiation of flat subduction (Model "zfab" in Table 1). Effective viscosity field is shown within an enlarged 1100 × 385 km domain of the original 4000 × 670 km model. Black arrows show the calculated velocity field. Colors represent the magnitude of the effective viscosity (as in the colorbar). Time (Myr) of shortening is given in the figures. The inset images show the composition fields for the same domain with white numbered isothermal lines in °C.

density and second invariants of the deviatoric strain rate and stress fields).

In the steep subduction mode, the continental margin subducts to >100 km depth following the high-angle oceanic subduction channel (Fig. 6a). Significant characteristics include the detachment of subducting upper/middle crust at the entrance zone of the subduction channel, with a series of thrust faults formed (Fig. 6a,b). A small amount of crustal rocks located in the lower part of the channel are detached from the plate at asthenospheric depths, indenting into the mantle wedge and forming a compositionally buoyant plume (Fig. 6b). Such sublithospheric plumes are discussed in detail in Currie et al. (2007) and Li and Gerya (2009). In addition, a partially molten plume forms in the deeply subducted oceanic plate and moves up vertically until it collapses at the bottom of the overriding lithospheric mantle (Fig. 6b,c). As subduction continues, another partially molten plume forms in the deeply subducted continental plate. It also moves up vertically until it collapses at the bottom of the overriding lithospheric mantle (Fig. 6c). The characteristics and 2-D and 3-D dynamics of this kind of plume are studied in detail in Gerya and Yuen (2003b) and Zhu et al. (2009).

As continental subduction continues, partially molten rocks accumulated in the subduction channel extrude upward to crustal depths (Fig. 6b, c). Then these UHP rocks exhume buoyantly to the surface to form a dome structure (Fig. 6c). The exhumed UHP rocks are mainly located near the suture zone with a fold-thrust belt formed in the foreland extending for about 300–400 km (Fig. 6c). P–T paths (Fig. 6, inset) show that peak P–T conditions of the exhumed rocks are 2.5–4 GPa and 600–800 °C, respectively (also see Fig. S8 for the peak pressure and temperature conditions of the collision zone). This indicates the UHP metamorphic rocks are formed and exhumed from a depth >100 km.

### 3.3. Parameter sensitivity study

#### 3.3.1. Variable convergence velocity for the reference flat subduction model

The reference flat subduction model with an initial dip angle ($\theta$) of 10° (Model "zfab", Table 1) is further investigated with higher convergence velocity (Model "zfba", Table 1) and lower convergence velocity (Model "zfbb", Table 1). All the other parameters are the same as in Tables S2 and S3.

In the fast convergence regime (Model "zfba", Table 1), the oceanic and continental plates subduct and indent flatly into the bottom of the overriding lithosphere. A "rollback" structure is formed at the leading edge of the subducting plate (Fig. 7a,b), which is similar to the reference flat subduction model (Fig. 3). After the convergence ceases (1500 km shortening, ~15 Myr), the flatly subducted continental crustal rocks are partially molten, and then extrude upward to the surface forming a small dome structure (Fig. 7c,d). P–T paths (Fig. 7) show that peak P–T conditions of the exhumed rocks are 2.5–4 GPa and
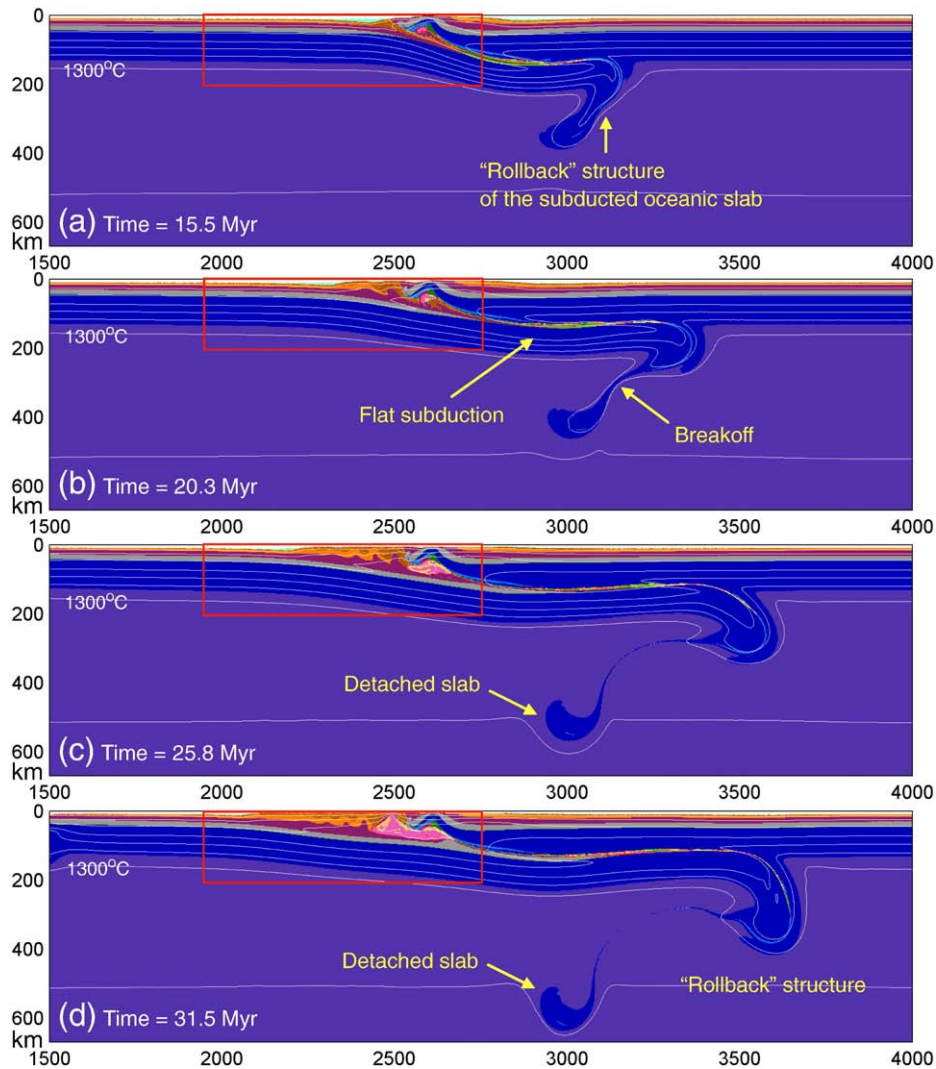
**Fig. 3.** Large scale evolution of the reference flat subduction model (Model "zfab" in Table 1) within an enlarged 2500 × 670 km domain of the original 4000 × 670 km model. Colors of rock types are as in Figure 1. Time (Myr) of shortening is given in the figures. White numbered lines are isotherms in °C.

600–800 °C, respectively (also see Fig. S9 for the peak pressure and temperature conditions of the collision zone).

In the slow convergence regime (Model "zfbb", Table 1), the oceanic plate subducts with the overriding plate deformed and bent (Fig. 8a). A two-sided subduction zone is formed (c.f. Faccenda et al., 2008), in which both plates subduct together (Fig. 8b). The oceanic upper crust from the subducting (left) plate is scraped off and exhumed (Fig. 8a,b). The edge of the overriding (right) plate detaches and remains in the collision zone, which can be considered as the suture zone between these two convergent plates (Fig. 8a–d). The subducted partially molten rocks exhume to the crustal level forming an UHP dome in the left side of the suture zone (Fig. 8c,d). In addition, partially molten middle/lower crust is present in the right side of the suture zone (Fig. 8c,d). P–T paths (Fig. 8) indicate that peak P–T conditions of the exhumed rocks in the left side of the channel are 2.5–4 GPa and 700–800 °C, respectively (also see Fig. S10 for the peak pressure and temperature conditions of the two-sided subduction/collision zone).

### 3.3.2. Variable convergence velocity for the reference steep subduction model

The reference steep subduction model with an initial dip angle ($\theta$) of 30° (Model "zfae", Table 1) is further investigated with higher convergence velocity (Model "zfca", Table 1) and lower convergence velocity (Model "zfcb", Table 1). All the other parameters are the same as in Tables S2 and S3.

In the fast convergence regime (Model "zfca", Table 1), the continental domain continues subducting along the high-angle oceanic subduction channel to the bottom of the lithospheric mantle (Fig. S11a). Then the crustal rocks in the lower part of the channel detach from the plate at asthenospheric depths, intrude into the mantle wedge, and form a horizontal compositionally buoyant plume (Fig. S11a–c). In addition, a partially molten plume forms in the deeply subducted plate and moves up vertically until it collapses at the bottom of the overriding lithospheric mantle (Fig. S11c,d), which is similar to behavior of the reference steep subduction model. After the convergence ceases (1500 km shorting, ~15 Myr), the subducted continental crustal rocks in the sub-lithospheric plume extrude upward to the surface forming a dome structure (Fig. S11d). P–T paths (Fig. S11) indicate that peak P–T conditions of the exhumed rocks are 3–4 GPa and 600–800 °C, respectively (also see Fig. S12 for the peak pressure and temperature conditions of the collision zone).

In the slow convergence regime (Model "zfcb", Table 1), the continental margin also subducts to >100 km depth along the high-angle oceanic subduction channel to the bottom of the lithospheric mantle (Fig. S13a). A small amount of crustal rocks located in the lower part of channel detaches from the plate and forms a compositionally
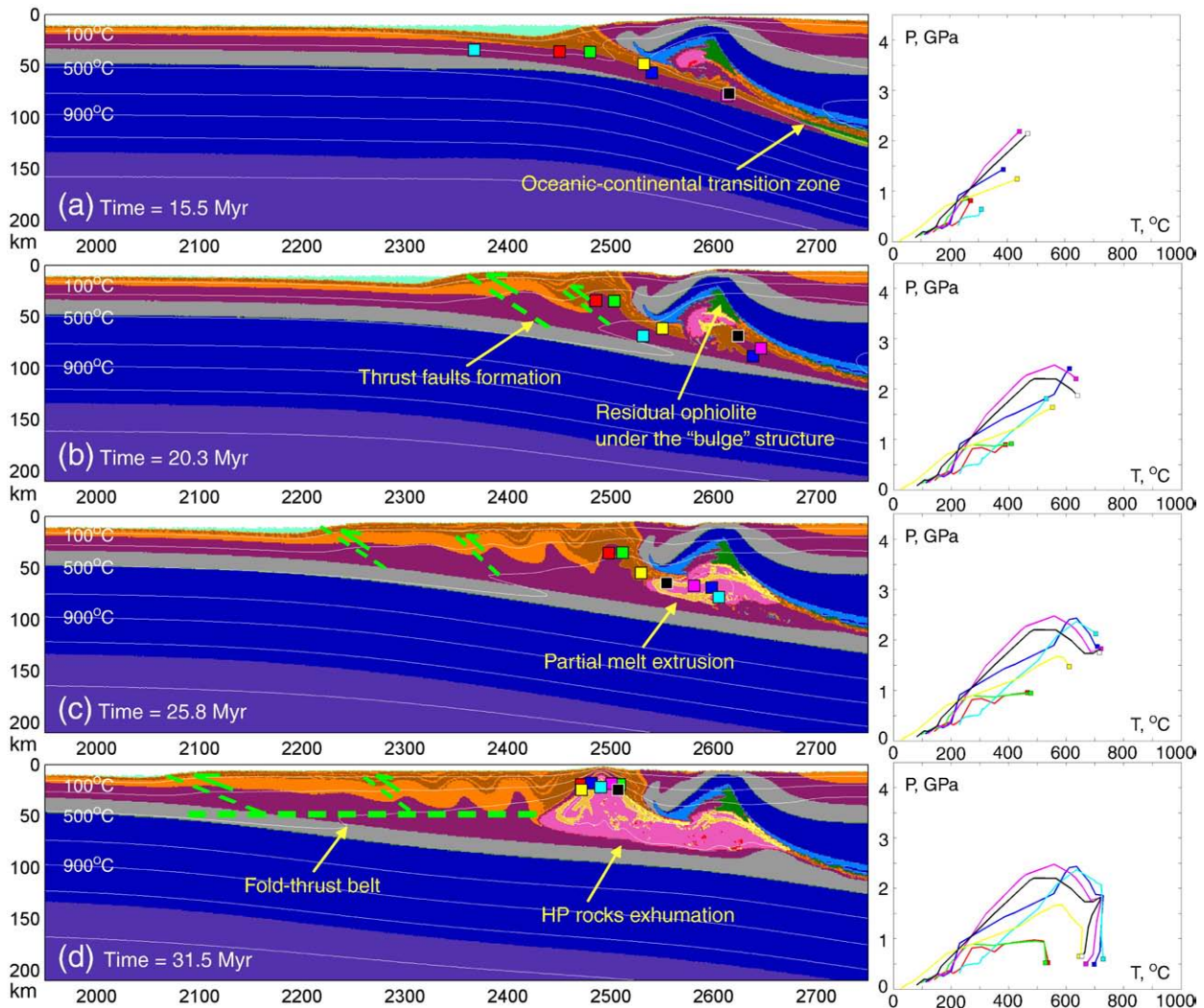
**Fig. 4.** Enlarged domain evolution (800×210 km as red rectangles indicated in Fig. 3) of the reference flat subduction model (Model "zfab" in Table 1). Colors of rock types are as in Figure 1. Time (Myr) of shortening is given in the figures. White numbered lines are isotherms in °C. Small colored squares indicate positions of representative markers (rock units) for which P–T paths are shown (right). Colors of these squares are used for discrimination of marker points plotted in P–T diagrams and do not correspond to the colors of rock types.

buoyant plume (Fig. S13a,b). The subducting upper/middle crust at the entrance zone of the subduction channel detaches with thrust faults formed (Fig. S13a–d). With continued continental subduction, partially molten rocks accumulated in the subduction channel extrude upward to the crustal depth (Fig. S13c,d). P–T paths (Fig. S13) show that peak P–T conditions of the exhumed rocks are 2–4 GPa and 600–800 °C (also see Fig. S14 for the peak pressure and temperature conditions of the collision zone).

Parameter sensitivity studies indicate that the convergence velocity can significantly influence the subduction and exhumation styles of the flat subduction model. It results in either one-sided (Fig. 7) or two-sided (Fig. 8) subduction. By contrast, in the steep subduction regime it only changes the amount of crustal rocks subducted to and exhumed from UHP depth (c.f. Figs. S11–S12 and Figs. S13–S14). As discussed in the Introduction, many factors may influence the subduction/collision styles as well as the exhumation of HP–UHP rocks. Therefore we also investigate the sensitivity to other parameters, e.g. initial thermal structure of the oceanic lithosphere (Appendix A.2 and Figs. S15–S18).

## 4. Geological implications for the Himalayan collisional belt

The Himalayan range is one of the largest, latest and best documented continental collisional belts, and provides significant constraints on subduction/collision processes due to the many geological (e.g., DiPietro and Pogue, 2004; Kind et al., 2002; Leech et al., 2005; Royden et al., 2008; Tapponnier et al., 2001; Yin, 2006, 2009) and geophysical/seismological data available (e.g., Li et al., 2008; Nabelek et al., 2009; Negredo et al., 2007; Van der Voo et al., 1999).

The Himalayan belt evolved mainly by the subduction/collision of the Indian continental plate beneath/with the Asian continent, following the earlier Tethyan oceanic subduction (e.g., Argand, 1924; Beaumont et al., 1994; Bird, 1978; Mattayer, 1986; Molnar, 1988). There are many plausible models for the absorption of Indian lithosphere in the collision zone (e.g., from the previously-mentioned geological and geophysical investigations). One of them is under-thrusting (flat subduction), first proposed by Argand (1924) and later supported by many others (e.g., Nelson et al., 1996; Owens and Zandt, 1997; Zhou and Murphy, 2005). Another possible model suggests that the Indian lithospheric plate, with its crust scraped off, plunges steeply into the asthenosphere (e.g., Mattayer, 1986; Negredo et al., 2007; Replumaz et al., 2004). The non-unique interpretation of tomographic images of the Himalayan and Tibetan regions might arise from insufficient resolution of the data and complexity of the actual deep structure (e.g., Oreshin et al., 2008). One possible process may be a hybrid (temporal and/or spatial) of the seemingly incompatible models. Chemenda et al. (2000) and Leech et al. (2005) proposed that
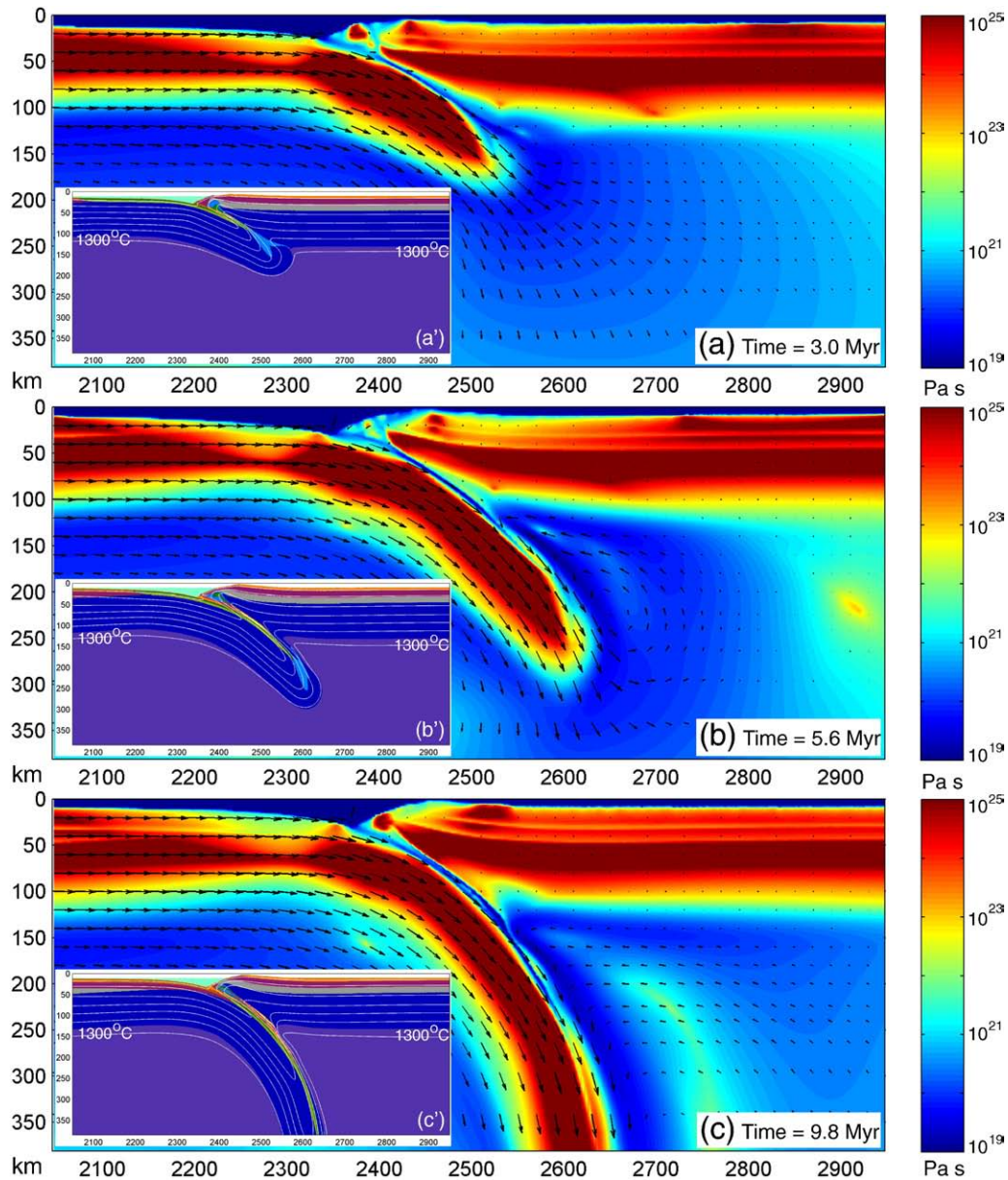
**Fig. 5.** Initiation of steep subduction (Model "zfae" in Table 1). Effective viscosity field is shown within enlarged 900 × 385 km domain of the original 4000 × 670 km model. Black arrows show the calculated velocity field. Colors represent the magnitude of effective viscosity (as in the colorbar). Time (Myr) of shortening is given in the figures. The inset images show the composition fields of the same domain with white numbered isothermal lines in °C. Note the small scale convection in the mantle wedge in (b).

Indian subduction was steep at the beginning and then flat after slab break-off. On the other hand, Guillot et al. (2008) and Oreshin et al. (2008) argued that the Indian subduction modes (flat or steep) may be different in different parts of the Himalayan belt.

HP and UHP rocks with origins in a variety of protoliths occur in various settings related to the Tethyan and Indian subduction beneath Asia: accretionary wedge, oceanic subduction zone, subducted continental margin and continental collisional zone (e.g. Guillot et al., 2008). Based on the summary of these HP–UHP rocks in Himalaya (Fig. 9), it reveals that UHP rocks are found exclusively in western Himalaya (Kaghan massif and Tso Morari massif); while in the extensional central Himalaya only HP rocks are found, mainly along the Indus Tsangpo suture zone. Guillot et al. (2008) proposed a plausible geodynamical model for the initial subduction of the Indian continental margin during the Paleocene–Eocene. In the central Himalaya, flat subduction leads to the underthrusting of the Indian slab beneath southern Tibet producing only HP rocks. In the western Himalaya, by contrast, steep subduction of

the Indian continental crust results in the formation and exhumation of UHP rocks. In our numerical models, the reference steep subduction model (Fig. 6) produces much higher peak pressure metamorphic rocks exhumed to the surface, compared to the reference flat subduction model (Fig. 4). The peak temperature values are more or less the same (c.f. Figs. 6 and 4). However the peak temperature metamorphic rocks in the steep subduction model are more widely distributed than in the flat subduction model (c.f. Figs. S8b and S4b).

### 4.1. Comparison of the reference flat subduction model with central Himalaya

In the central Himalaya, most geophysical profiles show that the Indian plate dips flatly beneath southern Tibet with a maximum crustal depth of 80 km, indicating the flat (low-angle) subduction mode (e.g., Huang et al., 2000; Nabelek et al., 2009; Nelson et al., 1996; Owens and Zandt, 1997; Schulte-Pelkum et al., 2005; Zhou and Murphy, 2005).
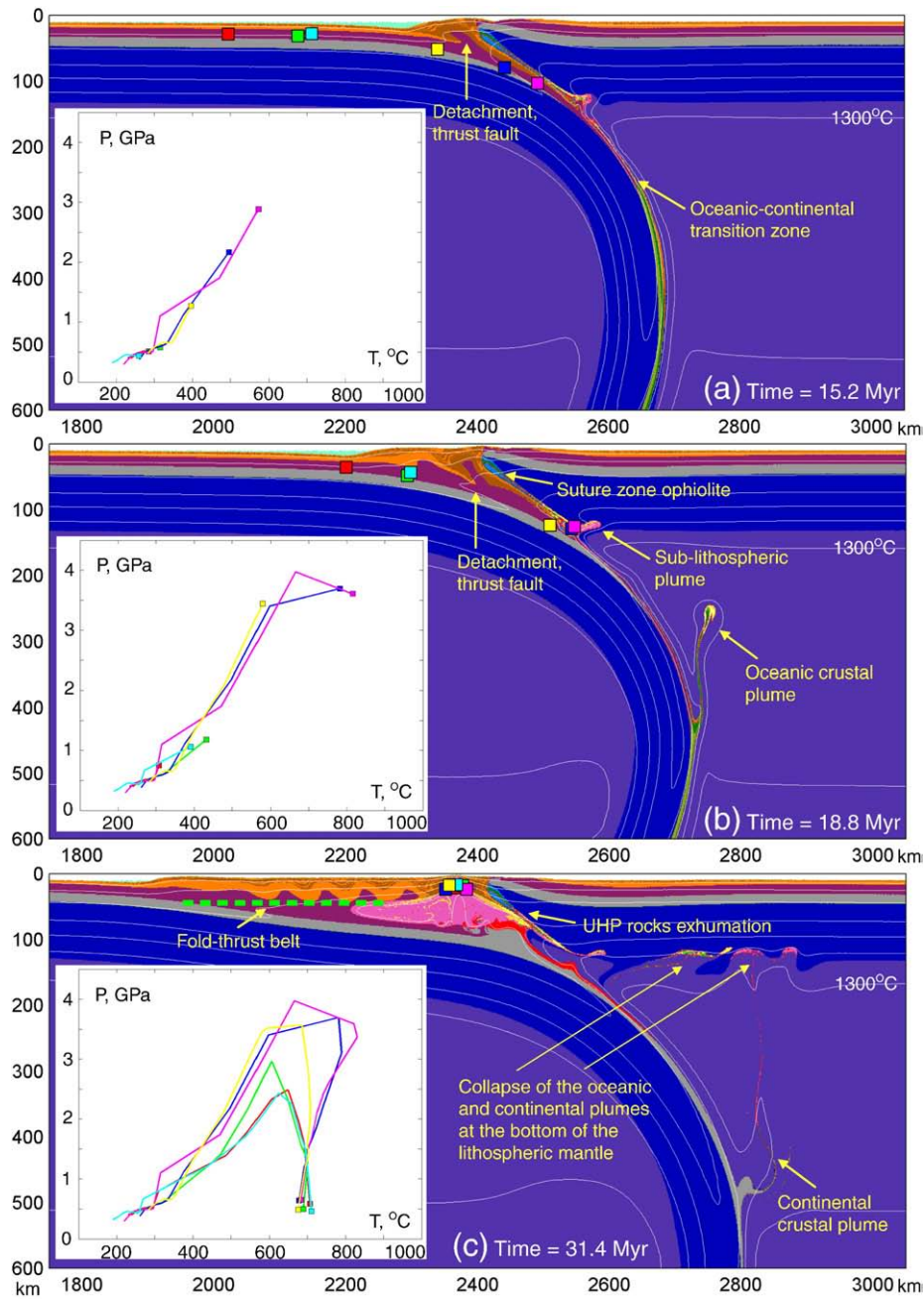
**Fig. 6.** Enlarged domain evolution (1300×600 km) of the reference steep subduction model (Model "zfae" in Table 1). Colors of rock types are as in Figure 1. Time (Myr) of shortening is given in the figures. White numbered lines are isotherms in °C. Small colored squares indicate positions of representative markers (rock units) for which *P–T* paths are shown (inset). Colors of these squares are used for discrimination of marker points plotted in *P–T* diagrams and do not correspond to the colors of rock types.

In the extensional central Himalaya, several HP units are found (Fig. 9). However coesite-bearing UHP rocks have never been reported (e.g., Guillot et al., 2008). In the flat subduction model (Fig. 4) the subducted crustal rocks can only extrude/exhume from <80 km depth forming HP units in the surface, which is consistent with the central Himalaya. In addition, the flat subduction model (Figs. 3 and 4) shares a number of other general characteristics with the main central Himalayan range, e.g. "rollback" structure of the subducted slab (e.g., van der Voo et al., 1999), a detached lithospheric remnant (e.g., van der Voo et al., 1999) and series of thrust faults in the foreland (e.g., Yin, 2006).

In summary, the flat subduction model is consistent with many observations in the central Himalaya, including the deep structure from most of the geophysical profiles, the absence of UHP rocks, and the crustal structure of the foreland. However it is worth emphasizing that flat subduction is not always the necessary condition for the absence of exhumation of UHP rocks, because the burial and exhumation of UHP rocks are constrained by many factors, e.g. rheological strength of the crust, convergence rate etc.

### 4.2. Comparison of the reference steep subduction model with the western Himalaya

In the western Himalaya, most tomographic images and seismic studies indicate steep (high angle) subduction beneath the Hindu Kush (e.g., Negredo et al., 2007; Roecker, 1982; Van der Voo et al., 1999).

The presence of UHP rocks is well documented in the Kaghan and Tso Morari massifs, western Himalaya. The protoliths of both massifs
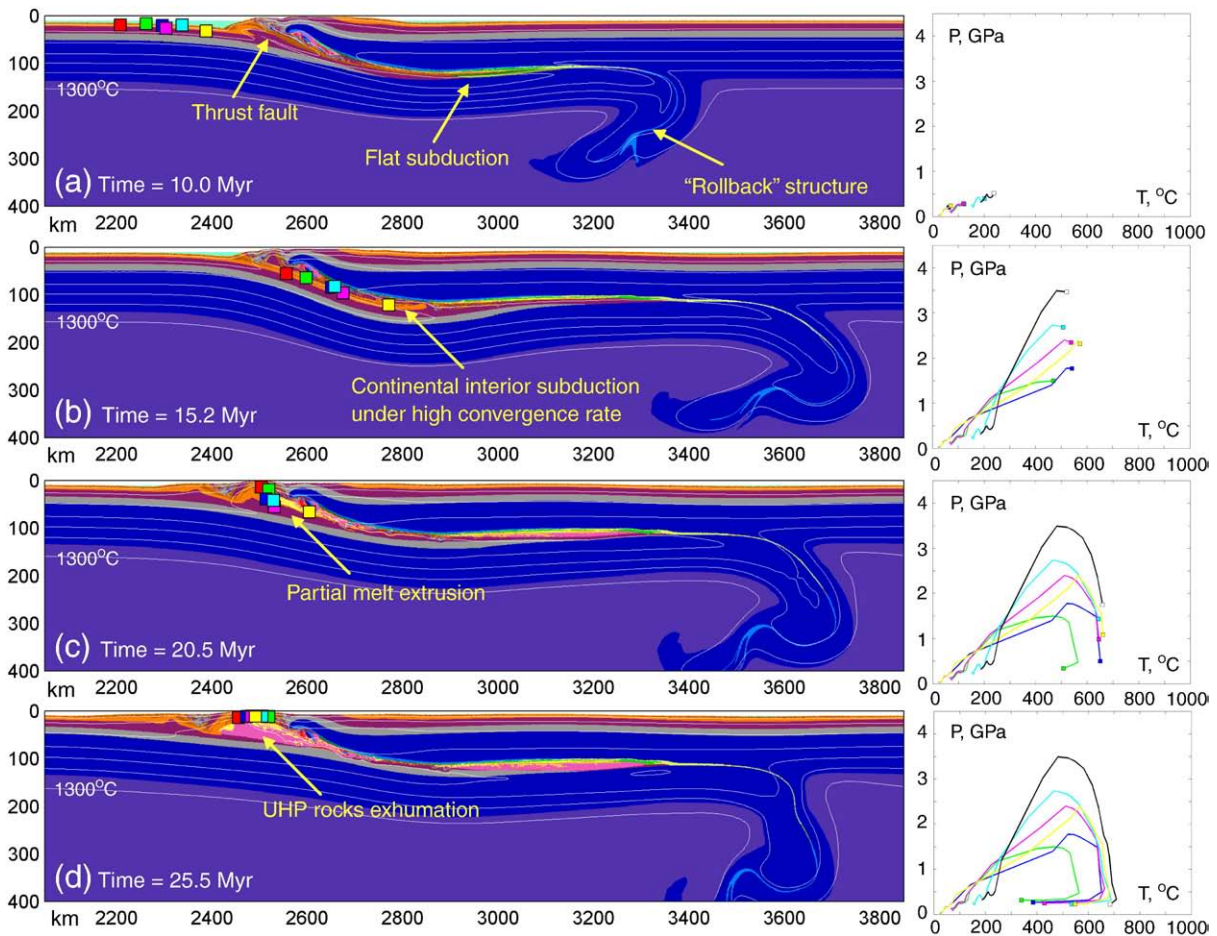
**Fig. 7.** Enlarged domain evolution (1800 × 400 km) of the model with higher convergence velocity and low initial dip angle (Model "zfba" in Table 1). Colors of rock types are as in Figure 1. Time (Myr) of shortening is given in the figures. White numbered lines are isotherms in °C. Small colored squares indicate positions of representative markers (rock units) for which *P–T* paths are shown (right). Colors of these squares are used for discrimination of marker points plotted in *P–T* diagrams and do not correspond to the colors of rock types.

originate from the continental margin of the Indian plate (e.g., Guillot et al., 2008). For the Kaghan massif, peak metamorphic conditions for coesite-bearing unit are estimated at 3.0 ± 0.2 GPa and 770 ± 50 °C (O'Brien et al., 2001) and coesite-free unit at 2.4 ± 0.2 GPa and 610 ± 30 °C (Lombardo et al., 2000). For the Tso Morari massif, Mukheerjee et al. (2003, 2005) suggested peak *P–T* conditions of >3.5 GPa and >750 °C. These data indicate subduction down to a depth>100 km, followed by exhumation. Several HP units are also found in the western Himalaya along the suture zone (Fig. 9).

The numerical models show that steep oceanic subduction (Fig. 6; see also Figs. S11–S14) can lead to deep subduction of the continental margin with formation and exhumation of UHP rocks in the continental collision zone. Model results are consistent with the UHP units in the western Himalaya: (1) UHP rocks are located near the suture zone as a dome structure (e.g., Epard and Steck, 2008); (2) rock types are mainly from upper/middle continental margin crust; and (3) peak *P–T* conditions are 2.5–4 GPa and 600–800 °C (Fig. 6).

### 4.3. UHP rocks extrusion in the (flat) faster convergence model

In the (flat) faster convergence model, the continental interior can also subduct to >100 km depth (Fig. 7a,b). The extrusion and exhumation processes occur after convergence ceases (Fig. 7c,d). A limited quantity of UHP rocks is finally extruded to the surface (Fig. 7; also see Fig. S9).

Guillot et al. (2003) suggested that the Himalayan shortening velocity is 18 cm yr$^{-1}$ in oceanic subduction (>55 Ma), 18–2.5 cm yr$^{-1}$

in continental subduction (55–50 Ma), 2.5–2.0 cm yr$^{-1}$ in continental collision (50–25 Ma) and ~2.0 cm yr$^{-1}$ in steady state collision (25–0 Ma). In this case, the convergence velocity decreases sharply from a very high value (18 cm yr$^{-1}$) to a low value (2.5 cm yr$^{-1}$) in the stage of continental margin subduction. This indicates that a high average convergence velocity of 10 cm yr$^{-1}$ used for the subduction/collision in the numerical models (e.g., Fig. 7) is also acceptable. So the (flat) faster convergence model (Fig. 7) is applicable to yield implications for the initial Himalayan collision.

### 4.4. Differential continental subduction modes in the same collisional belt?

The previously-mentioned comparisons and discussions favor a spatially differential subduction/collision model for the Himalayan range, which is further supported by the fact that the western Himalaya is clearly distinct from the central Himalaya in structural, petrological and metamorphic characteristics (Fig. 9). In the western Himalaya, steep subduction dominates, whereas flat subduction dominates in the extensional central Himalaya, resulting in a concentration of HP–UHP rocks in the western Himalaya.

The initial geometry and kinematics of the Greater Indian plate as well as the time of collision onset with the Asian continent are obscure and extensively debated (e.g., Ali and Aitchinson, 2005; Guillot et al., 2003). A significant inference is that Indian continental margin subducted earlier in the western Himalaya than in the central Himalaya (e.g., Rowley, 1996; Treloar and Coward, 1991). Based on
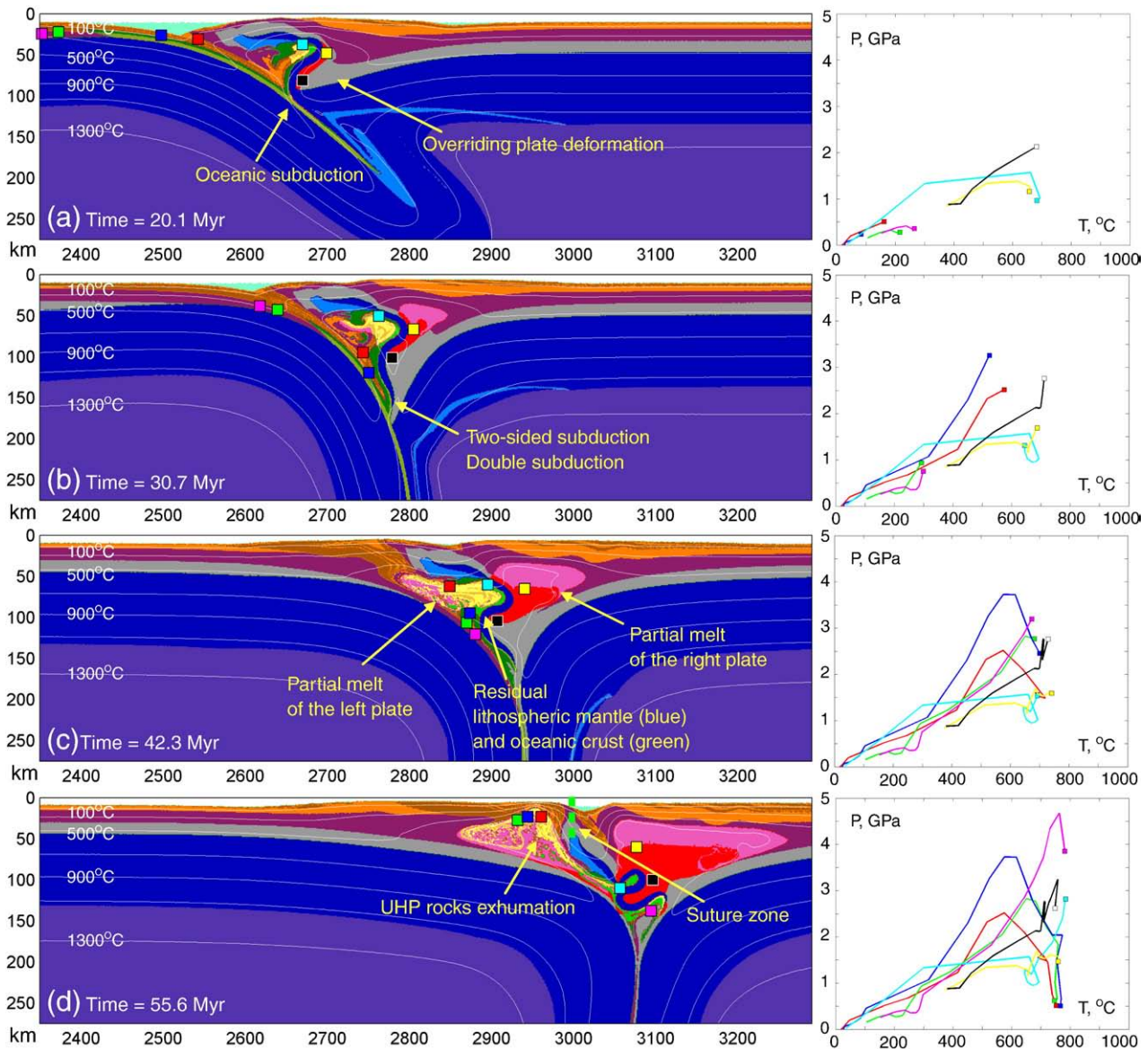
**Fig. 8.** Enlarged domain evolution (940×275 km) of the model with lower convergence velocity and low initial dip angle (Model "zfbb" in Table 1). Colors of rock types are as in Figure 1. Time (Myr) of shortening is given in the figures. White numbered lines are isotherms in °C. Small colored squares indicate positions of representative markers (rock units) for which P–T paths are shown (right). Colors of these squares are used for discrimination of marker points plotted in P–T diagrams and do not correspond to the colors of rock types.

this inference and our numerical results, another possible model for the distribution of HP–UHP rocks in the Himalaya is the temporally differential subduction/collision model. Flat subduction with high convergence velocity (early in time) occurred in the western Himalaya. As a result, the crustal rocks can be subducted to UHP depth and then exhumed from there after the decreased velocity or cessation of subduction. In contrast, flat subduction with relatively low convergence velocity (late in time) occurred in the central Himalaya. Consequently only HP rocks can be formed and exhumed to the surface.

The spatially and temporally differential subduction/collision models are both plausible. While the spatially differential model (steep subduction in the west and flat subduction in the central Himalaya) is consistent with the present-day slab geometry (from most of the tomographic images) and the distribution of HP–UHP rocks. By contrast, the temporally differential model (fast flat subduction in the west and relatively slow flat subduction in the central Himalaya) is mainly based on the general inferences of the initial geometry and kinematics of the Greater Indian plate, the

discrepant time of collision onset with the Asian continent, and the present-day distribution of HP–UHP rocks.

## 5. Discussion

### 5.1. Why slab dip angle controls (U)HP exhumation

Numerical simulations show that the dip angle of the initial weak zone ("seed") can result in either a flat or steep subduction style. If the weak seed has a low angle (e.g., 10° in Figs. 2–4), the high interplate hydrostatic suction (e.g., Gutscher et al., 2000b; Shemenda, 1993) results in strongly coupled plates, which will further lead to flat subduction. In this case, crustal materials of the subducting plate take a longer path (and time) to be subducted to a given depth compared to steep subduction (c.f. different depths of the oceanic/continental transition zone in Figs. 4a and 6a). During the long flat subduction process, the subducting crust will be heated and weakened. As a result, it detaches and exhumes before subducting to UHP depth (Fig. 4). However if the convergence velocity is much higher, flat
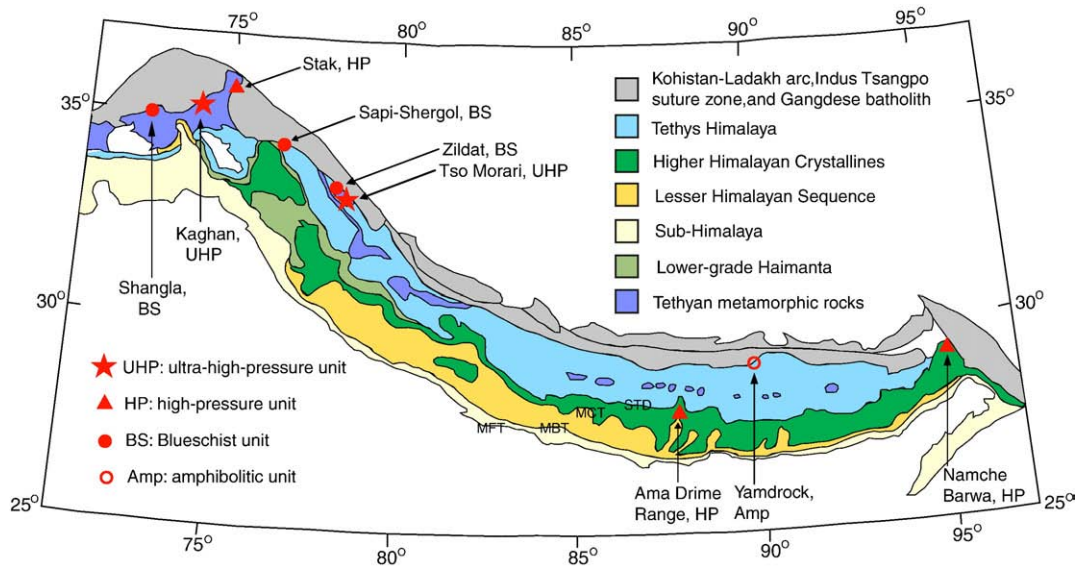
**Fig. 9.** Geological setting of the Himalayan collisional belt (after Ding et al., 2001; Di Pietro and Pogue, 2004; Guillot et al., 2003, 2008; Zhang et al., 2007; Yang et al., 2009). The red symbols (star, triangle, filled and empty circles) show the locations of the metamorphic units related to the oceanic/continental subduction processes.

subduction can also result in formation and exhumation of UHP rocks (Fig. 7).

In the models with a high angle weak seed (e.g. 30° in Figs. 5 and 6), the interplate hydrostatic suction is relatively low. Together with the decoupling effect of small scale convection in the mantle wedge, steep subduction is formed. In this case, crustal materials can subduct to UHP depths before being strongly weakened (Fig. 6). Consequently steep subduction can easily lead to exhumation of UHP rocks.

It is also worth noting that most of the exhumed HP–UHP rocks are partially molten in the numerical models. One reason is that the densities of partially molten rocks are lower than those of solid rocks (Tables S2 and S3), so that partially molten crustal rocks are easier to exhume. On the other hand, the rheological strength of partial molten rocks decreases with increasing melt fractions (see Equation 8 in Appendix A1.2; see also different rheological flow laws for solid and molten rocks in Tables S2 and S3). Therefore partially molten rocks have lower density and lower viscosity in the numerical implementations, which contribute greatly to the exhumation process.

### 5.2. Interplate interaction and overriding plate deformation

In the plate convergence zones, subducting and overriding plates interact with each other through different kinds of processes. In the reference flat subduction model (Figs. 3 and 4), underthrusting of the subducted cold lithosphere decreases the temperature under the overriding lithosphere. The converging plates are highly coupled together forming lithosphere whose thickness is nearly doubled. Similar styles and characteristics occur in the (flat) faster convergence model (Fig. 7).

In the steep subduction model, the interactions between plates are mainly based on the plumes (Fig. 6). Three types of plumes are produced in the numerical models (Fig. 6): sub-lithospheric plumes formed by indenting of subducted crustal rocks into the bottom of the overriding lithosphere (Fig. 6b), partially molten plumes originating from the subducted oceanic plate (Fig. 6b) and partially molten plumes originating from the subducted continental plate (Fig. 6c). These plumes destabilize the thermal structure as well as the material field at the bottom of the overriding lithospheric mantle (Fig. 6), which leads to the thinning of the lithosphere. Later, it may contribute to produce lithospheric plumes in the overriding plate (not produced

in our model). The variable convergence velocities of steep subduction model result in plumes of different sizes (c.f. Figs. 6, S11 and S13).

The slower convergence of the reference flat subduction model results in two-sided subduction (also called double subduction) and formation of a thick and narrow symmetrical collisional zone (Fig. 8). Due to the weakening effect of shear heating, changes in convergence velocity strongly modify the rheological coupling at the plate interface. This coupling seems to be the most important parameter that influences the style of post-subduction collisional orogeny (Faccenda et al., 2008; Willingshofer and Sokoutis, 2009) because it determines the magnitude of shearing forces applied to the overriding plate and, consequently, the extent of ablation of the lithospheric material. The term "ablation" is used in the sense of the original definition in Tao and O'Connell (1992), to describe the downward dragging of the lithospheric material due to viscous shearing imposed by the down-going plate. In their case the rate of ablation is a function of plate buoyancy. In addition, the numerical results in Faccenda et al. (2008) show that the rate of ablation also depends strongly on the magnitude of coupling and on the strength of the crust. Frictional heating produced at the shearing interface influences coupling — for low velocities where small stress/strain values are achieved, a huge amount of lithosphere of the overriding plate is tectonically eroded (Fig. 8). On the other hand, high velocities produce high shear heating so that the slabs are almost completely detached and only a small portion of the overriding continental lithosphere is dragged downward (Fig. 7).

### 5.3. Upper crustal structure of the HP–UHP terranes

In both the flat and steep subduction models, the general characteristics are the formation of series of thrust faults, which are initiated at and migrate from the entrance zone of the subduction channel in the foreland direction (e.g., Figs. 4 and 6). Finally a fold-thrust belt will be formed in the foreland of the subduction/collision zone (Figs. 4d and 6c). This kind of foreland structure is well-documented in the Dabie–Sulu HP–UHP collisional belt in eastern China (e.g., Faure et al., 2003; Hacker et al., 1998, 2000).

In addition, as summarized in Beaumont et al. (2009), the upper-crustal settings of many UHP terranes share a number of structural characteristics: (1) a dome structure cored by the UHP nappe, (2) domes flanked by low-grade accretionary wedge and/or upper crustal sedimentary rocks, (3) overlying and underlying medium- to high-

pressure nappes, (4) suture zone ophiolites and (5) foreland-directed thrust faults and the syn-exhumation normal faults. Our numerical models reproduce the general characteristic upper crustal structures, especially the dome structure of the HP–UHP cores, the flanked and overlaid low-grade accretionary wedge, the foreland-directed thrust faults and the fold-thrust belt. The ophiolites are distributed near the suture zone in the steep subduction model (Fig. 6), whereas the ophiolites in the flat subduction model are located under the bulge of the overriding plate (Fig. 4).

## 6. Conclusions

Numerical models show that the subduction angle plays an important role in controlling both continental collision modes and the metamorphic conditions of HP–UHP rocks. In the reference flat subduction model, the two converging plates are highly coupled with only HP rocks exhumed to the surface. In the reference steep subduction model, by contrast, the two plates are less coupled and UHP rocks are formed and exhumed. In addition, faster convergence of the reference flat subduction model produces extrusion of UHP rocks after the cessation of convergence. Slower convergence of the reference flat subduction model results in two-sided subduction/collision and formation of a thick and narrow symmetrical collisional zone. The higher/lower convergence velocities of the reference steep subduction model can both produce exhumation of UHP rocks.

Based on our numerical results, especially those concerning the metamorphic conditions of HP–UHP rocks, we propose two possible models for the subduction and collision styles of the Himalaya range: (1) A spatially differential subduction/collision model, according to which steep subduction dominates in the western Himalaya, whereas flat subduction dominates in the extensive central Himalaya. (2) A temporally differential subduction/collision model, according to which the continental plate (flatly) subducted earlier with high convergence velocity in the western Himalaya, while it (flatly) subducted later with relatively low convergence velocity in the central Himalaya. Consequently the HP–UHP rocks are mainly found in the western Himalaya.

Supplementary materials related to this article can be found online at doi:10.1016/j.epsl.2010.10.014.

## References

Abbott, D., Drury, R., Smith, W.H.F., 1994. Flat to steep transition in subduction style. Geology 22, 937–940.
Ali, J.R., Aitchison, J.C., 2005. Greater India. Earth Sci. Rev. 72, 169–188.
Argand, E., 1924. La tectonque de l'Asie. Proc. Int. Geol. Cong. 7, 171–372.
Bird, P., 1978. Initiation of intracontinental subduction in the Himalaya. J. Geophys. Res. 83, 4975–4987.
Beaumont, C., Fullsack, P., Hamilton, J., 1994. Styles of crustal deformation in compressional orogens caused by subduction of the underlying lithosphere. Tectonophysics 232, 119–132.
Beaumont, C., Jamieson, R.A., Nguyen, M.H., Lee, B., 2001. Himalayan tectonics explained by extrusion of a low-viscosity crustal channel coupled to focused surface denudation. Nature 414, 738–742.
Beaumont, C., Jamieson, R.A., Butler, J.P., Warren, C.J., 2009. Crustal structure: a key constraint on the mechanism of ultra-high-pressure rock exhumation. Earth Planet. Sci. Lett. 287, 116–129.
Bittner, D., Schmeling, H., 1995. Numerical modeling of melting processes and induced diapirism in the lower crust. Geophys. J. Int. 123, 59–70.

Boutelier, D., Chemenda, A.I., Jorand, C., 2004. Continental subduction and exhumation of high-pressure rocks: insights from thermo-mechanical laboratory modeling. Earth Planet. Sci. Lett. 222, 209–216.
Burg, J.-P., Gerya, T.V., 2005. The role of viscous heating in Barrovian metamorphism of collisional orogens: thermomechanical models and application to the Lepontine Dome in the Central Alps. J. Metamorph. Geol. 23, 75–95.
Burov, E., Jolivet, L., Le Pourhiet, L., Poliakov, A., 2001. A thermomechanical model of exhumation of high pressure (HP) and ultra-high pressure (UHP) metamorphic rocks in Alpine-type collision belts. Tectonophysics 342, 113–136.
Chemenda, A.I., Mattauer, M., Malavieille, J., Bokun, A., 1995. A mechanism for syn-collisional rock exhumation and associated normal faulting: results from physical modeling. Earth Planet. Sci. Lett. 132, 225–232.
Chemenda, A.I., Mattauer, M., Bokun, A., 1996. Continental subduction and a mechanism for exhumation of high-pressure metamorphic rocks: new modelling and field data from Oman. Earth Planet. Sci. Lett. 143, 178–182.
Chemenda, A.I., Burg, J.-P., Mattauer, M., 2000. Evolutionary model of the Himalaya–Tibet system: geopoem based on new modelling, geological and geophysical data. Earth Planet. Sci. Lett. 174, 397–409.
Clauser, C., Huenges, E., 1995. Thermal conductivity of rocks and minerals. In: Ahrens, T. J. (Ed.), Rock Physics and Phase Relations. American Geophysical Union, Reference Shelf 3, Washington D.C, pp. 105–126.
Currie, C.A., Beaumont, C., Huismans, R.S., 2007. The fate of subducted sediments: a case for backarc intrusion and underplating. Geology 35 (12), 1111–1114.
Ding, L., Zhong, D., Yin, A., Kapp, P., Harrison, T.M., 2001. Cenozoic structural and metamorphic evolution of the eastern Himalayan syntaxis (Namche Barwa). Earth Planet. Sci. Lett. 192, 423–438.
DiPietro, J.A., Pogue, K.R., 2004. Tectonostratigraphic subdivisions of the Himalaya: a view from the west. Tectonics 23, TC5001, doi:10.1029/2003TC001554.
Epard, J.-L., Steck, A., 2008. Structural development of the Tso Morari ultra-high pressure nappe of the Ladakh Himalaya. Tectonophysics 451, 242–264.
Espurt, N., Funiciello, F., Martinod, J., Guillaume, B., Regard, V., Faccenna, C., Brusset, S., 2008. Flat subduction dynamics and deformation of the South American plate: Insights from analog modeling. Tectonics 27, TC3011, doi:10.1029/2007TC002175.
Faccenda, M., Gerya, T.V., Chakraborty, S., 2008. Styles of post-subduction collisional orogeny: influence of convergence velocity, crustal rheology and radiogenic heat production. Lithos 103, 257–287.
Faure, M., Lin, W., Scharer, U., Shu, L., Sun, Y., Arnaud, N., 2003. Continental subduction and exhumation of UHP rocks: structural and geochronological insights from the Dabieshan (East China). Lithos 70, 213–241.
Gerya, T.V., Stöckhert, B., Perchuk, A.L., 2002. Exhumation of high-pressure metamorphic rocks in a subduction channel: a numerical simulation. Tectonics 21 (6), 1056, doi:10.1029/2002TC001406.
Gerya, T.V., Yuen, D.A., 2003a. Characteristics-based marker-in-cell method with conservative finite-differences schemes for modeling geological flows with strongly variable transport properties. Phys. Earth Planet. Inter. 140, 293–318.
Gerya, T.V., Yuen, D.A., 2003b. Rayleigh–Taylor instabilities from hydration and melting propel cold plumes at subduction zones. Earth Planet. Sci. Lett. 212, 47–62.
Gerya, T.V., Stöckhert, B., 2006. Two-dimensional numerical modeling of tectonic and metamorphic histories at active continental margins. Int. J. Earth Sci. 95, 250–274.
Gerya, T.V., Perchuk, L.L., Burg, J.-P., 2008. Transient hot channels: perpetrating and regurgitating ultrahigh-pressure, high-temperature crust–mantle associations in collision belts. Lithos 103, 236–256.
Guillot, S., Garzanti, E., Baratoux, D., Marquer, D., Mahéo, G., de Sigoyer, J., 2003. Reconstructing the total shortening history of the NW Himalaya. Geochem. Geophys. Geosyst. 4 (1), doi:10.1029/2002GC000484.
Guillot, S., Mahéo, G., de Sigoyer, D., Hattori, K.H., Pêcher, A., 2008. Tethyan and Indian subduction viewed from the Himalayan high- to ultrahigh-pressure metamorphic rocks. Tectonophysics 451, 225–241.
Gutscher, M.-A., Maury, R., Eissen, J.-P., Bourdon, E., 2000a. Can slab melting be caused by flat subduction? Geology 28 (6), 535–538.
Gutscher, M.-A., Spakman, W., Bijwaard, H., Engdahl, E.R., 2000b. Geodynamics of flat subduction: seismicity and tomographic constraints from the Andean margin. Tectonics 19 (5), 814–833.
Hacker, B.R., Ratschbacher, L., Webb, L., Ireland, T., Walker, D., Dong, S., 1998. U/Pb zircon ages constrain the architecture of the ultrahigh-pressure Qinling–Dabie Orogen, China. Earth Planet. Sci. Lett. 161, 215–230.
Hacker, B.R., Ratschbacher, L., Webb, L., McWilliams, M.O., Ireland, T., Calvert, A., Dong, S., Wenk, H.-R., Chateigner, D., 2000. Exhumation of ultrahigh-pressure continental crust in east central China: Late Triassic–Early Jurassic tectonic unroofing. J. Geophys. Res. 105 (B6), 13339–13364.
Huang, W.-C., Ni, J.F., Tilmann, F., Nelson, D., Guo, J., Zhao, W., Mechie, J., Kind, R., Saul, J., Rapine, R., Hearn, T.M., 2000. Seismic polarization anisotropy beneath the central Tibetan Plateau. J. Geophys. Res. 105 (B12), 27979–27989.
Ji, S., Zhao, P., 1993. Flow laws of multiphase rocks calculated from experimental data on the constituent phases. Earth Planet. Sci. Lett. 117, 181–187.
Kind, R., Yuan, X., Saul, J., Nelson, D., Sobolev, S.V., Mechie, J., Zhao, W., Kosarev, G., Ni, J., Achauer, U., Jiang, M., 2002. Seismic images of crust and upper mantle beneath Tibet: evidence for Eurasian plate subduction. Science 298, 1219–1221.
Kirby, S.H., 1983. Rheology of the lithosphere. Rev. Geophys. Space Phys. 21, 1458–1487.
Kirby, S.H., Kronenberg, A.K., 1987. Rheology of the lithosphere: selected topics. Rev. Geophys. 25, 1219–1244.
Labrosse, S., Jaupart, C., 2007. Thermal evolution of the Earth: secular changes and fluctuations of plate characteristics. Earth Planet. Sci. Lett. 260, 465–481.
Lallemand, S., Heuret, A., Boutelier, D., 2005. On the relationships between slab dip, back-arc stress, upper plate absolute motion, and crustal nature in subduction zones. Geochem. Geophys. Geosyst. 6 (9), Q09006, doi:10.1029/2005GC000917.

Leech, M.L., Singh, S., Jain, A.K., Klemperer, S.L., Manickavasagam, R.M., 2005. The onset of India–Asia continental collision: early, steep subduction required by the timing of UHP metamorphism in the western Himalaya. Earth Planet. Sci. Lett. 234, 83–97.

Li, C., van der Hilst, R.D., Meltzer, A.S., Engdahl, E.R., 2008. Subduction of the Indian lithosphere beneath the Tibetan Plateau and Burma. Earth Planet. Sci. Lett. 274, 157–168.

Li, Z., Gerya, T.V., 2009. Polyphase formation and exhumation of HP–UHP rocks in continental subduction zone: numerical modelling and application to the Sulu UHP terrane in eastern China. J. Geophys. Res. 114, B09406, doi:10.1029/2008JB005935.

Li, Z.H., Gerya, T.V., Burg, J.P., 2010. Influence of tectonic overpressure on P–T paths of HP–UHP rocks in continental collision zones: thermomechanical modelling. J. Metamorph. Geol. 28, 227–247.

Liou, J.G., Tsujimori, T., Zhang, R.Y., Katayama, I., Maruyama, S., 2004. Global UHP metamorphism and continental subduction/collision: the Himalayan model. Int. Geol. Rev. 46, 1–27.

Lombardo, B., Rolfo, F., Compagnoni, R., 2000. Glaucophane and barroisite eclogites from the upper Kaghan Nappe; implications for the metamorphic history of the NW Himalaya. In: Khan, M.A., Treloar, P.J., Searle, M.P., Jan, M.Q. (Eds.), Tectonics of the Nanga Parbat Syntaxis and the Western Himalaya: Geol. Soc. Spec. Pub., 170, pp. 411–430.

Martinod, J., Funiciello, F., Faccenna, C., Labanieh, S., Regard, V., 2005. Dynamical effects of subducting ridges: insights from 3-D laboratory models. Geophys. J. Int. 163, 1137–1150.

Mattayer, M., 1986. Intracontinental subduction, crust–mantle decollement and crustal stacking wedge in the Himalayas and other collisional belts. In: Coward, M.P., Ries, A.C. (Eds.), Collision Tectonics: Geol. Soc. Lond. Spec. Pub., No. 19, pp. 37–50.

Molnar, P., 1988. A review of geophysical constraints on the deep structure of the Tibetan Plateau, the Himalaya and the Karakoram, and their tectonic implications. Philos. Trans. R. Soc. Lond. A 326, 33–88.

Mukherjee, B., Sachan, H.K., Ogasa   waray, Y., Muko, A., Yoshioka, N., 2003. Carbonate-bearing UHPM rocks from the Tso-Morari Region, Ladakh, India: petrological implications. Int. Geol. Rev. 45, 49–69.

Mukherjee, B., Sachan, H.K., Ahmad, T., 2005. A new occurrence of microdiamond from Indus Suture zone, Himalata: a possible origin. In: Memoire, H.S. (Ed.), Special extended Abstract Volume: Géologie Alpine, 44, p. 136.

Nabelek, J., Hetenyi, G., Vergne, J., Sapkota, S., Kafle, B., Jiang, M., Su, H., Chen, J., Huang, B.-S., the Hi-CLIMB Team, 2009. Underplating in the Himalaya–Tibet collision zone revealed by the Hi-CLIMB experiment. Science 325, 1371–1374.

Negredo, A.M., Replumaz, A., Villasenor, A., Guillot, S., 2007. Modeling the evolution of continental subduction processes in the Pamir–Hindu Kush region. Earth Planet. Sci. Lett. 259, 212–225.

Nelson, K.D., Zhao, W., Brown, L.D., Kuo, L., Che, J., Liu, X., Klemperer, S.L., Makovsky, Y., Meissner, R., Mechie, J., Kind, R., Wenzel, F., Ni, J., Nabelek, J., Chen, L., Tan, H., Wei, W., Jones, A.G., Booker, J., Unsworth, M., Kidd, W.S.F., Hauck, M., Alsdorf, D., Ross, A., Cogan, M., Wu, C., Sandvol, E., Edwards, M., 1996. Partial molten middle crust beneath southern Tibet: Synthesis of project INDEPTH results. Science 274, 1684–1688.

O'Brien, P., Zotov, N., Law, R., Khan, A.M., Jan, M.Q., 2001. Coesite in Himalayan eclogite and implication for models of India–Asia collision. Geology 29, 435–438.

Oreshin, S., Kiselev, S., Vinnik, L., Prakasamb, K.S., Rai, S.S., Makeyeva, L., Savvin, Y., 2008. Crust and mantle beneath western Himalaya, Ladakh and western Tibet from integrated seismic data. Earth Planet. Sci. Lett. 271, 75–87.

Owens, T.J., Zandt, G., 1997. Implications of crustal property variations for models of Tibetan plateau evolution. Nature 387, 37–43.

Pope, D., Willett, C., 1998. Thermal–mechanical model for crustal thickening in the central Andes driven by ablative subduction. Geology 26 (6), 511–514.

Ranalli, G., Murphy, D.C., 1987. Rheology stratification of the lithosphere. Tectonophysics 132, 281–295.

Ranalli, G., 1995. Rheology of the Earth, Deformation and Flow Processes in Geophysics and Geodynamics, second ed. Chapman & Hall.

Replumaz, A., Karason, H., van der Hilst, R.D., Besse, J., Tapponnier, P., 2004. 4-D evolution of SE Asia's mantle from geological reconstructions and seismic tomography. Earth Planet. Sci. Lett. 221, 103–115.

Roecker, S.W., 1982. Velocity structure of the Pamir–Hindu Kush region: possible evidence of subducted crust. J. Geophys. Res. 87 (B2), 945–959.

Rowley, D.B., 1996. Age of initiation of collision between India and Asia: a review of stratigraphic data. Earth Planet. Sci. Lett. 145, 1–13.

Royden, R.H., Burchfiel, B.C., van der Hilst, R.D., 2008. The geological evolution of the Tibetan Plateau. Science 321, 1054–1058.

Schmidt, M.W., Poli, S., 1998. Experimentally based water budgets for dehydrating slabs and consequences for arc magma generation. Earth Planet. Sci. Lett. 163, 361–379.

Schulte-Pelkum, V., Monsalve, G., Sheehan, A., Pandey, M.R., Sapkota, S., Bilham, R., Wu, F., 2005. Imaging the Indian subcontinent beneath the Himalaya. Nature 435, 1222–1225.

Shemenda, A.I., 1993. Subduction of the lithosphere and back arc dynamics: insights from physical modelling. J. Geophys. Res. 98 (B9), 16167–16185.

Stöckhert, B., Gerya, T.V., 2005. Pre-collisional high pressure metamorphism and nappe tectonics at active continental margins: a numerical simulation. Terra Nova 17, 102–110.

Tao, W., O'Connell, R., 1992. Ablative subduction: a two-sided alternative to the conventional subduction model. J. Geophys. Res. 97 (B6), 8877–8904.

Tapponnier, P., Xu, Z., Roger, F., Meyer, B., Arnaud, N., Wittlinger, G., Yang, J., 2001. Oblique stepwise rise and growth of the Tibet Plateau. Science 294, 1671–1677.

Toussaint, G., Burov, E., Jolivet, L., 2004a. Continental plate collision: unstable vs. stable slab dynamics. Geology 32 (1), 33–36.

Toussaint, G., Burov, E., Avouac, J.-P., 2004b. Tectonic evolution of a continental collision zone: a thermomechanical numerical model. Tectonics 23, TC6003, doi:10.1029/2003TC001604.

Treloar, P.J., Corward, M.P., 1991. Indian Plate motion and shape: constraints on the geometry of the Himalayan orogen. Tectonophysics 191, 189–198.

Turcotte, D.L., Schubert, G., 1982. Geodynamics: Application of Continuum Physics to Geological Problems. New York, John Wiley, p. 450.

Turcotte, D.L., Schubert, G., 2002. Geodynamics, second ed. Cambridge Univ, Press.

Van Hunen, J., van den Berg, A.P., Vlaar, N.J., 2002a. The impact of the South-American plate motion and the Nazca Ridge subduction on the flat subduction below South Peru. Geophys. Res. Lett. 29 (14), 1690, doi:10.1029/2001GL014004.

Van Hunen, J., van den Berg, A.P., Vlaar, N.J., 2002b. On the role of subducting oceanic plateaus in the development of shallow flat subduction. Tectonophysics 352, 317–333.

Van Hunen, J., van den Berg, A.P., Vlaar, N.J., 2004. Various mechanisms to induce shallow flat subduction: a numerical parameter study. Phys. Earth Planet. Inter. 46, 179–194.

Van der Voo, R., Spakman, W., Bijwaard, H., 1999. Tethyan subducted slabs under India. Earth Planet. Sci. Lett. 171, 7–20.

Vlaar, N.J., 1983. Thermal anomalies and magmatism due to lithospheric doubling and shifting. Earth Planet. Sci. Lett. 65, 322–330.

Vlaar, N.J., 1985. Precambrian geodynamical constraints. In: Tobi, A.C., Touret, J.L.R. (Eds.), The Deep Proterozoic Crust in North Atlantic Provinces. Reidel Publ. Co, pp. 3–20.

Warren, C.J., Beaumont, C., Jamieson, R.A., 2008a. Modelling tectonic styles and ultra-high pressure (UHP) rock exhumation during the transition from oceanic subduction to continental collision. Earth Planet. Sci. Lett. 267, 129–145.

Warren, C.J., Beaumont, C., Jamieson, R.A., 2008b. Formation and exhumation of ultra-high pressure rocks during continental collision: role of detachment in the subduction channel. Geochem. Geophys. Geosyst. 9 (4), Q04019, doi:10.1029/2007GC001839.

Willingshofer, E., Sokoutis, D., 2009. Decoupling along plate boundaries: key variable controlling the mode of deformation and the geometry of collisional mountain belts. Geology 37, 39–42.

Yamato, P., Agard, P., Burov, E., Le Pourhiet, L., Jolivet, L., Tiberi, C., 2007. Burial and exhumation in a subduction wedge: mutual constraints from thermomechanical modeling and natural P–T–t data (Schistes Lustres, western Alps). J. Geophys. Res. 112, B07410, doi:10.1029/2006JB004441.

Yamato, P., Burov, E., Agard, P., Le Pourhiet, L., Jolivet, L., 2008. HP–UHP exhumation during slow continental subduction: self-consistent thermodynamically and thermomechanically coupled model with application to the Western Alps. Earth Planet. Sci. Lett. 271, 63–74.

Yang, J.S., Xu, Z.Q., Zhang, J.S., Zhang, Z.M., Liu, F.L., Wu, C.L., 2009. Tectonic setting of main high- and ultrahigh-pressure metamorphic belts in China and adjacent region and discussion on their subduction and exhumation mechanism. Acta Petrol. Sin. 25 (7), 1529–1560.

Yin, A., 2006. Cenozoic tectonic evolution of the Himalayan orogen as constrained by along-strike variation of structural geometry, exhumation history, and foreland sedimentation. Earth Sci. Rev. 76, 1–131.

Yin, A., 2009. Cenozoic tectonic evolution of Asia: a preliminary synthesis. Tectonophysics, doi:10.1016/j.tecto.2009.06.002.

Zhang, Z.M., Zheng, L.L., Wang, J.L., Zhao, X.D., Shi, C., 2007. Garnet pyroxenite in the Namjagbarwa Group-complex in the eastern Himalayan tectonic syntaxis, Tibet, China: evidence for subduction of the Indian continent beneath the Eurasian plate at 80–100 km depth. Geol. Bull. China 26 (1), 1–12.

Zhou, H.-W., Murphy, M., 2005. Tomographic evidence for whole scale underthrusting of India beneath the entire Tibetan plateau. J. Asian Earth Sci. 25, 445–457.

Zhu, G., Gerya, T.V., Yuen, D.A., Honda, S., Yoshida, T., Connolly, J.A.D., 2009. 3-D dynamics of hydrous thermal–chemical plumes in oceanic subduction zones. Geochem. Geophys. Geosyst. 10, Q11006, doi:10.1029/2009GC002625.